“Quantized” Doping of Individual Colloidal Nanocrystals Using Size-Focused Metal Quantum Clusters

Beatriz Santiago-González†, Angelo Monguzzi†, Valerio Pinchetti†, Alberto Casu⊥, Mirko Prato‡, Roberto Lorenzi†, Marcello Campione§, Norberto Chiodini†, Carlo Santambrogio∥, Francesco Meinardi†, Liberato Manna⊥, and Sergio Brovelli†*

† Dipartimento di Scienza dei Materiali, Università degli Studi di Milano-Bicocca, Via R. Cozzi 55, IT-20125 Milano, Italy

‡ Materials Characterization Facility, Istituto Italiano di Tecnologia, Via Morego 30, IT-16163 Genova, Italy

§ Dipartimento di Scienze dell'Ambiente e della Terra, Università degli Studi di Milano-Bicocca, Piazza della Scienza 4, IT-20126 Milano, Italy

∥ Dipartimento di Biotecnologie e Bioscienze, Università degli Studi di Milano-Bicocca Piazza della Scienza 2, IT-20126 Milano, Italy

⊥ Nanochemistry Department, Istituto Italiano di Tecnologia, Via Morego 30, IT-16163 Genova, Italy

**E-mail: sergio.brovelli@unimib.it*

Abstract

The insertion of intentional impurities, commonly referred to as doping, into colloidal semiconductor quantum dots (QDs) is a powerful paradigm for tailoring their electronic, optical, and magnetic behaviors beyond what is obtained with size-control and heterostructuring motifs. Advancements in colloidal chemistry have led to nearly atomic precision of the doping level in both lightly and heavily doped QDs. The doping strategies currently available, however, operate at the ensemble level, resulting in a Poisson distribution of impurities across the QD population. To date, the synthesis of monodisperse ensembles of QDs individually doped with an identical number of impurity atoms is still an open challenge, and its achievement would enable the realization of advanced QD devices, such as optically/electrically controlled magnetic memories and intragap state transistors and solar cells, that rely on the precise tuning of the impurity states (i.e., number of unpaired spins, energy and width of impurity levels) within the QD host. The only approach reported to date relies on QD seeding with organometallic precursors that are intrinsically unstable and strongly affected by chemical or environmental degradation, which prevents the concept from reaching its full potential and makes the method unsuitable for aqueous synthesis routes. Here, we overcome these issues by demonstrating a doping strategy that bridges two traditionally orthogonal nanostructured material systems, namely, QDs and metal quantum clusters composed of a “magic number” of atoms held together by stable metal-to-metal bonds. Specifically, we use clusters composed of four copper atoms (Cu4) capped with d-penicillamine to seed the growth of CdS QDs in water at room temperature. The elemental analysis, performed by electrospray ionization mass spectrometry, X-ray fluorescence, and inductively coupled plasma mass spectrometry, side by side with optical spectroscopy and transmission electron microscopy measurements, indicates that each Cu:CdS QD in the ensemble incorporates four Cu atoms originating from one Cu4 cluster, which acts as a “quantized” source of dopant impurities.

Colloidal semiconductor quantum dots (QDs), (1, 2) prized for their tunable electronic and optical properties, solution-phase processability, and size monodispersity, are gaining growing interest in various optoelectronic and photonic devices including light-emitting diodes, (3-5) photovoltaic cells, (6) electronic transistors, (7) lasers, (8) sensors, (9, 10) and, more recently, luminescent solar concentrators. (11-14) In addition to this, advancements in QD surface chemistry (15) and functionalization with biomolecules are boosting their use as target-specific labels in bioimaging and nanodiagnostics. (10, 16, 17) Tunability of the electronic properties of QDs is typically achieved by control of the particle size (*quantum confinement effect*) (18, 19) and by so-called wave function engineering of heteronanostructures. (20-24) Doping with transition metal (25-27) or lanthanide (28-30) ions provides additional degrees of freedom for obtaining technologically relevant functionalities that are difficult to realize with other design motifs, such as a large “real” Stokes shift between the emission and the absorption spectra, (11, 31, 32) long emission lifetimes, (31) two-color luminescence, (33) para- and photomagnetism, (34-37) and enhanced electrical behaviors. (38, 39)

Generally, the doping of QDs is performed following three main strategies, conventionally named after the stage of the synthesis reaction at which the insertion of the doping impurity takes place: (i) nucleation doping, (40-42) in which an organometallic precursor containing the impurity atom (43, 44) is directly mixed with the host precursors prior to nucleation, so that doping occurs directly on the

adatom cores; (45) (ii) growth doping, (40, 42) where the dopant precursors are added to the reactive medium during the growth stage and gradually decorate the QD surfaces that are successively coated with layers of the same semiconductor material as the QD core through a homogeneous shelling reaction; (46, 47) (iii) cation exchange reactions between undoped QDs and dopant precursors. (39, 48, 49) In this case, the introduction of the impurities occurs after the completion of the QD synthesis, and the doping level is controlled by the relative concentration of QDs and the dopant source, as well as by the choice of ligands and reaction temperature. Cation exchange reactions can also be performed following the so-called "inverted" route, as in the case of Ag-doped CdSe QDs starting from Ag_2Se QDs, where the final doped systems are obtained by incomplete substitution of the Ag atoms with Cd ones, which leaves the inner core of the QDs doped with residual Ag impurities. (32) Similar to cation exchange reaction, but without the loss of host cations, "diffusion doping" has been demonstrated to successfully incorporate large amounts of manganese ions in CdSe QDs. (50, 51) Similarly, by reducing the size of the semiconductor host to the near minimum, subnanometer-sized Mn:ZnTe and Mn:CdSe clusters (49, 52) have been obtained with very high relative dopant concentration. Very recently, approaches have been proposed to realize diluted magnetic semiconductor QDs with uniform spatial distribution of impurities by synthesis of a small core containing magnetic ions followed by high-temperature annealing and growth of the semiconducting matrix. (53)

Remarkable advancements in the chemistry of QD doping and, in particular, in the knowledge of cation exchange reactions, have led to the achievement of nearly atomic precision of the doping level in both lightly and heavily doped QDs. (38, 48) Despite success in fine-tuning the average amount of impurities per particle, the common feature of the above-mentioned QD-doping approaches is that they operate at the ensemble level, yielding a Poisson distribution of dopants across the QD population. To date, the realization of monodisperse ensembles of QDs individually doped with an identical number of impurity atoms is still an open challenge, and its achievement would be highly important from both a fundamental and a technological perspective, as it would offer a platform for investigating the dopant-to-host and dopant-to-dopant interactions that are typically rendered inaccessible by the inhomogeneity in the doping concentration. (31, 35, 54) This will enable us to realize and control the behavior of quantum dot devices, such as optically/electrically controlled magnetic memories (54) and intragap state transistors and solar cells that rely on the precise tuning of the impurity states (*i.e.*, number of unpaired spins, energy and width of impurity levels, *etc.*) within the semiconductor host. (36, 55, 56)

An important step in this direction has been made by Snee and co-workers, (43) who used $[Na(H_2O)_3]_2[Cu_4(SPh)_6]$ organometallic precursors (57) to grow CdSe QDs doped with copper, indicating that monodispersity of the doping level across the QD ensemble can be achieved. The employed complexes, consisting of copper atoms

bridged by benzenethiols, were synthesized following a modified synthetic protocol introduced by Dance *etal*. (57) to obtain copper-based hybrid compounds to be employed as monodispersed dopant source. Despite success in overcoming the Poissonian distribution of dopants in the NC ensemble typical of other doping techniques, these metal complexes require manipulation under an inert atmosphere due to their low stability to decomposition and oxidation, which further makes them incompatible with synthesis procedures employing aqueous solvents.

Here, by taking inspiration from that pioneering study, we propose a quantized doping approach utilizing a different kind of pretuned dopant source that extends the potential of the original strategy and renders the synthesis procedure compatible with aqueous solvents and environmental conditions useful for direct application of QDs to biologic and sensing applications. (58-60) Specifically, we employ metal quantum clusters, consisting of a core of copper atoms held together by stable metal–metal bonds, to pretune the doping at the single-particle level and thereby obtain ensembles of doped QDs, each one of which is grown on the same predetermined number of impurity atoms. Metal quantum clusters are monodispersed ultrasmall particles typically synthesized in aqueous media and highly stable in saline, as well as biologic environments. (61, 62) They consist of a precise number of atoms that dictates their electronic properties, (63) which make them technologically appealing in nanomedicine, (61) electronics, (64) photocatalysis, (65) and photonics. (66) This

applicative potential has triggered growing efforts on their synthesis strategies, resulting in a variety of fabrication protocols for preparing clusters consisting of well-defined numbers of gold, (65-67) silver, (62, 68) and more recently copper atoms. (69) Besides their chemical and environmental stability, a general feature of metal quantum clusters that is particularly relevant for their use as atomically precise sources of metal impurities for QD doping is that, by using size-focusing methodologies, (70) they can be obtained with monodispersed "magic number" sizes dictated by the specific values of their nuclearity. (71) Finally, one important beneficial aspect of metal quantum clusters as tailored dopant sources is that they can be synthesized in both pure monometallic compositions and in a large variety of "alloyed" polymetallic forms, (72, 73) which, in principle, offers an unmatched platform for dual or multiple doping through direct incorporation of preset arrays of different metal impurities in the semiconductor host, simultaneously ensuring a controlled doping level of all impurities and thereby overcoming the ubiquitous difference in reactivity of mixtures of molecular dopant precursors.

In this study, in order to provide a direct comparison with the approach based on organometallic copper–benzenethiol complexes, we use monometallic metal clusters composed of four copper atoms (Cu_4) as nucleation seeds for cadmium sulfide (CdS) QDs in water, at room temperature and ambient atmosphere, and employ glutathione biomolecules as capping ligands, which might further promote their suitability to bioimaging and diagnostic applications. (74-76) The choice of

copper as dopant metal is also advantageous due to the consolidated knowledge of the electronic properties of Cu:doped II–VI QDs, which makes the identification of the spectroscopic signatures of copper doping unequivocal. (31, 34, 42, 77-79) The elemental analysis of the clusters and the doped QDs performed by electrospray ionization mass spectrometry (ESI-MS), X-ray fluorescence (XRF), and inductively coupled plasma mass spectrometry (ICP-MS), side by side with optical spectroscopy measurements, indicates that each Cu:CdS QD in the ensemble contains four copper atoms and confirms that the growth of the doped QDs is seeded by individual Cu_4 clusters, which act as a "quantized" source of dopant impurities. This is a fundamental difference with respect to approaches based on conventional doping sources that are typically incorporated in a variable number, leading to statistic distributions of the doping level across the ensemble. The obtained Cu:CdS QDs exhibit the typical spectroscopic properties of Cu:doped QDs synthesized *via* established nucleation and growth doping routes, (80) such as long-lived Stokes-shifted photoluminescence and insensitivity of the emission efficiency to hole-withdrawing agents, (34, 77) which further confirms the incorporation of the Cu dopants in the bulk of the host QD.

Results and Discussion

Synthesis and Characterization of Copper Clusters

The synthesis route consists of a two-step solution-based bottom-up procedure with the preparation of Cu_4 clusters followed by the nucleation of the CdS nanocrystals,

as schematized in Figure 1a. Monodisperse water-soluble Cu_4 clusters were synthesized using mild reducing conditions of $Cu(NO_3)_2$. Briefly, 40 µL of $Cu(NO_3)_2$ in water (100 mM) was added to 4 mL of the zwitterionic functional ligand D-penicillamine (DPA, 10 mM), which acts also as a mild reductant. The mixture was kept under vigorous stirring at room temperature for a few minutes, after which it turned turbid white due to the low solubility of the clusters in the reaction mixture at pH = 2.7. Accordingly, the solution showed the characteristic luminescence at ~640 nm (Figure 1b) with ~10 µs lifetime (Figure 1c), commonly ascribed to aggregation-induced emission copper clusters. (81) After 90 min, the clusters precipitated out of solution and were collected and purified by centrifugation and repeated washing with ultrapure water. The final product was redispersed in ultrapure water, yielding a clear solution with pH = 7.0 of noninteracting isolated Cu_4 clusters, as confirmed by the disappearance of the characteristic luminescence.

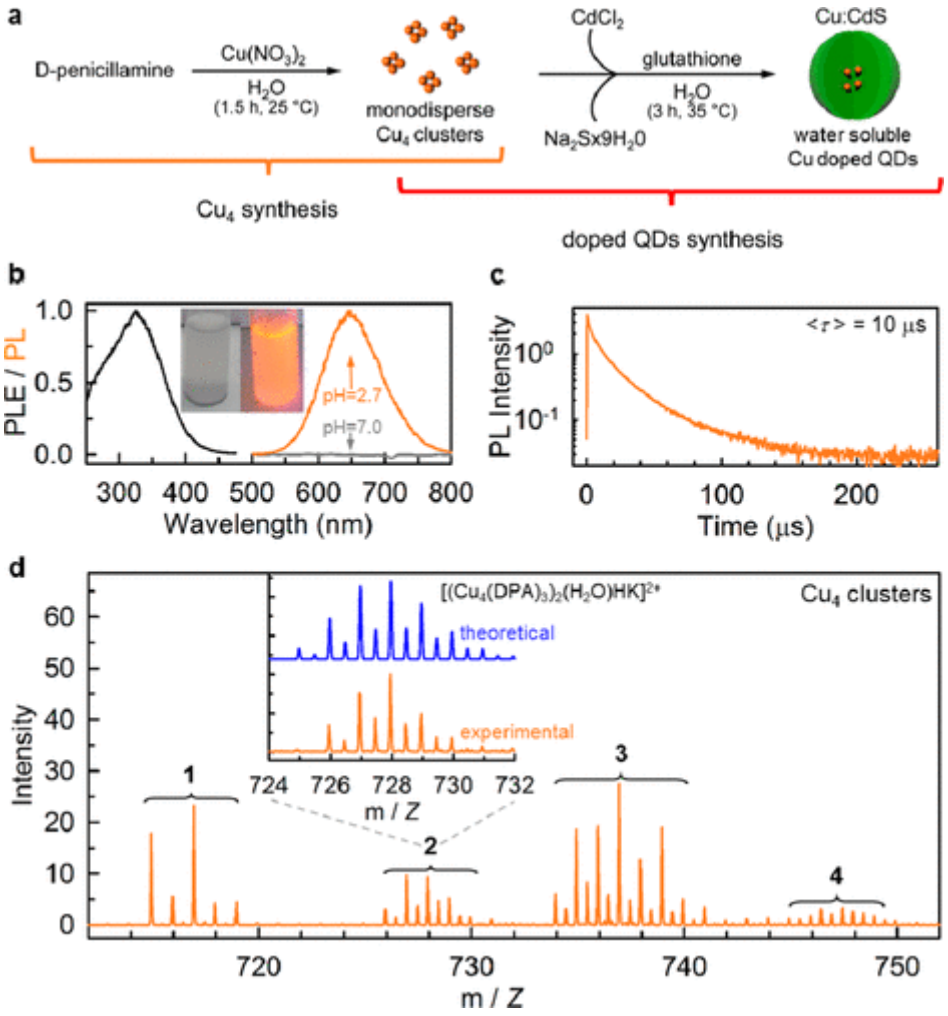

Figure 1. Synthesis and characterization of Cu_4 cluster seeds. (a) Schematics of the synthesis strategy of water-soluble copper quantum clusters. The copper clusters were prepared by chemical reduction of the metal precursor $Cu(NO_3)_2$ using ^{D}-penicillamine, which also acts as capping ligand. Cu-doped CdS QDs are obtained by seeding QD's nucleation through the addition of Cu clusters. (b) Photoluminescence (PL, orange line) and PL excitation (PLE, black line) spectra of Cu_4 clusters in water (pH = 2.7). (c) PL decay profile collected at 650 nm under pulsed 355 nm laser excitation. (d) Mass spectrum in positive-ion mode of copper clusters in water. All the recorded peaks (1, 2, 3, and 4) are ascribed to metal clusters composed of four Cu atoms. The details on the peak assignment are reported in Table S1. Inset:

Experimental and simulated isotopic patterns of peak 2 corresponding to [(Cu$_4$ (DPA)$_3$)$_2$(H$_2$O)HK]$^{2+}$.

To elucidate the size and monodispersity of the Cu clusters, ESI-MS measurements in positive-ion mode were carried out. The positive mode ESI-MS spectrum of the Cu clusters in water is reported in Figure 1d, showing a series of peaks in the *m*/*z* range between 710 and 755 that are ascribed to clusters composed of four Cu atoms capped by three DPA ligands. Specifically, the peaks are assigned to $[(Cu_4(DPA)_3)(H_2O)]^+$ (**1**, *m*/*z* = 716.52), $[(Cu_4(DPA)_3)_2(H_2O)HK]^{2+}$ (**2**, *m*/*z* = 727.84), $[(Cu_4(DPA)_3)_2\ (H_2O)_2HK]^{2+}$ (**3**, *m*/*z* = 736.91), and $[(Cu_4(DPA)_3)_2(H_2O)(K)_2]^{2+}$ (**4**, *m*/*z* = 746.74). The inset of Figure 1d reports the enlargement of peak 2, highlighting the isotopic pattern of the $[(Cu_4(DPA)_3)_2(H_2O)HK]^{2+}$ mass distribution. The experimental data match closely the corresponding simulated pattern calculated considering the isotopic distribution of the constituent atomic species (theoretical *m*/*z* = 727.85), thus confirming the formation of Cu_4 clusters capped by three DPA units. The same correspondence between the theoretical and experimental spectrum is found for all other peaks, as reported in Figure S1. We highlight that the ESI-MS spectrum in the 300–1500 *m*/*z* range shows no additional features, which confirms the absence of clusters of different size and of cluster aggregates, in agreement with the complete disappearance of the aggregation-induced luminescence. The oxidation state of the constituent copper atoms was investigated by X-ray photoelectron spectroscopy

(XPS) and by X-ray-induced Auger electron spectroscopy (XAES), which indicate that the clusters are mostly composed of Cu^{+} and Cu^{2+} ions (Figure S2).

Synthesis of Cu-Doped CdS Quantum Dots

Once thoroughly purified and characterized, the Cu_4 clusters were added to the cadmium and sulfur precursors in order to synthesize Cu_4-doped CdS QDs (Figure 1a). Prior to the preparation of doped QDs, undoped CdS QDs were synthesized using a modified version of the method in ref 82 to optimize the reaction parameters and to obtain preliminary guidelines on the Cu_4 cluster concentration required for producing a monodisperse ensemble of Cu-doped CdS QDs with the assumption, confirmed experimentally (see below), that each copper cluster seeds the nucleation of one single CdS QD. Specifically, 7 mL of 0.1 M tripeptide L-glutathione was added to 35 mL of ultrapure water in a two-necked flask under stirring and the pH was adjusted to 10 by dropwise addition of 1.0 M NaOH. Next, 350 µL of 0.1 M $CdCl_2$ was added to the mixture and stirred for 5 min, after which 350 µL of 0.1 M Na_2S was injected. The reaction temperature was fixed to 35 °C and the mixture was left to react for 3 h, after which the solution was purified using a 10 kDa centrifuge membrane to separate the QDs from the excess reactants. The obtained CdS QDs were characterized with high-resolution transmission electron microscopy (HR-TEM), X-ray diffraction (XRD), and optical spectroscopies, as discussed below (Figure 2). On the basis of the information gained, we proceeded with the synthesis of Cu:CdS QDs, following the same synthesis route, with the only

exception being the addition of a mild excess of Cu_4 clusters with respect to the concentration of the CdS precursors to the reaction medium, so as to ensure full doping of the whole QD ensemble. After a 3 h reaction, the solution was purified and concentrated by passing through a 10 kDa centrifuge filter to completely remove nonreacted Cu_4 clusters remaining in solution. Figure 2a reports representative HR-TEM images of the undoped and Cu-doped QDs together with the respective size histogram, which reveals similar sizes of the two QD ensembles, with an average size of ~3.8 ± 0.5 nm and ~3.8 ± 0.3 for the undoped and doped systems, respectively. The XRD patterns of both systems (Figure 2b) show the signature peaks of zincblende CdS, (83) indicating that the doping process does not alter the crystal structure of the QDs.

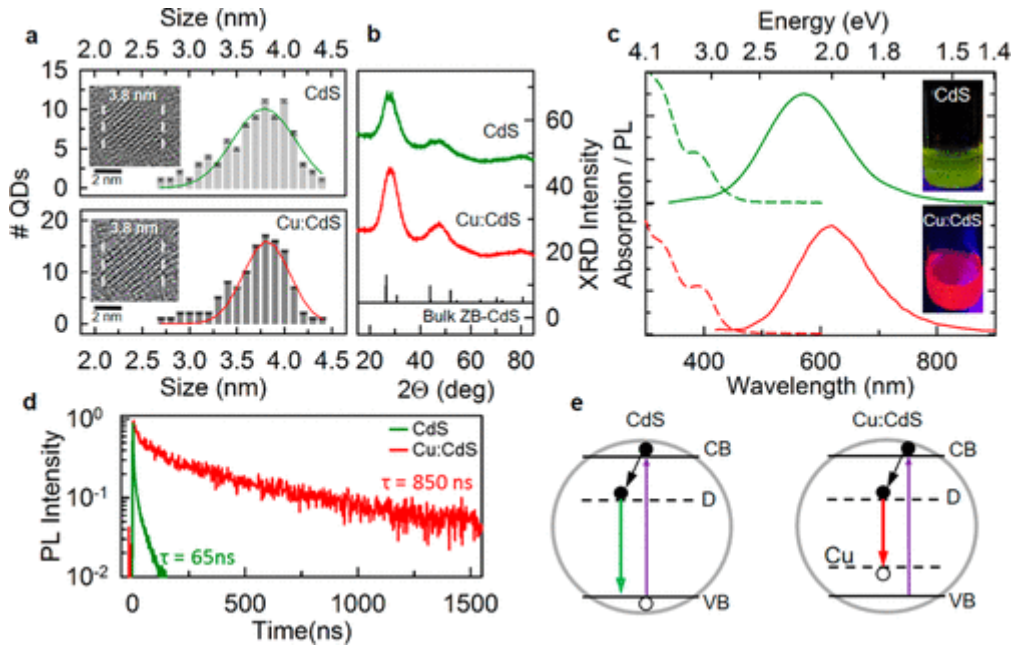

Figure 2. Structural and optical properties of undoped and Cu-doped water-soluble CdS QDs. (a) Size distribution and high-resolution transmission electron microscopy

(HR-TEM) images of undoped and copper-doped QDs, together with (b) the corresponding X-ray diffraction (XRD) patterns. The XRD pattern of bulk CdS in cubic zinc blende structure is reported as reference (black line). (c) Normalized absorption (dashed lines) and PL (solid lines) profiles of undoped CdS (green) and Cu:CdS QDs (red) in water. The insets show a photograph of the QD solutions under UV illumination. (d) Time-resolved photoluminescence of undoped (green line) and Cu:doped CdS under 405 nm pulsed excitation. (e) Schematic depiction of the recombination mechanism in undoped (left) and Cu:doped (right) QDs upon band-to-band excitation (violet arrows). The black arrows indicate the rapid localization of a conduction band (CB) electron in a localized state most likely associated with a surface defect (D). The recombination of the electron with a valence band (VB) hole in undoped QDs gives rise to the characteristic green defect luminescence (green arrow). The red arrow depicts the luminescence of doped QDs due to radiative decay of a photogenerated electron (represented as trapped in a surface state for consistency with the undoped QDs) in an intragap state associated with the Cu impurity.

Optical Properties of Undoped and Cu-Doped CdS Quantum Dots

The optical absorption and photoluminescence spectra of the two material systems are reported in Figure 2c, showing nearly identical absorption profiles, with a well-defined 1S absorption peak at 400 nm (∼3.1 eV), in good agreement with the expected energy gap of quantum-confined ∼4 nm particles observed by TEM. The

fwhm of the 1S peak is ∼0.26 eV and ∼0.25 eV for the doped and undoped QDs, respectively (Figure S3), confirming the good size homogeneity on the QD ensemble. Despite such similarities, undoped and Cu-doped QDs exhibit striking differences between their emission spectra and decay dynamics, deriving directly from the insertion of Cu atoms in the QD lattice. (31, 77, 79, 84) Specifically, undoped QDs show a broad luminescence peak at ∼550 nm (2.25 eV), with a characteristic lifetime of ∼65 ns (Figure 2d), consistent with the trap-mediated green emission commonly observed in unshelled CdS QDs synthesized in both aqueous and organic media (left scheme in Figure 2e). (82, 85-87)

In contrast, Cu-doped QDs show red luminescence at ∼610 nm (∼2.03 eV, Figure 2c) with a decay time of ∼850 ns (Figure 2d), which is over 10 times longer than the undoped counterparts and is consistent with the radiative relaxation of photoexcited electrons – either delocalized in the QD conduction band or trapped in shallow defects, as schematized in Figure 2e for consistency with the trap-assisted decay of undoped sample – in the localized intragap acceptor level associated with the d-states of the Cu impurities (right scheme in Figure 2e). (77, 79, 88) We highlight that the photoluminescence features of doped QDs are markedly different from those of aggregated Cu_4 clusters (Figure 1b,c) both in their spectral position and decay dynamics, which excludes a possible contribution from aggregated clusters left in solution despite the thorough purification process and the unfavorable pH that leads to their dissolution in nonemissive isolated species. We

also note that both doped and undoped QD samples show a fast initial decay component ascribed to surface trapping in surface defects, in agreement with the relatively low emission efficiency of both systems (Φ = 4.5 ± 0.4%) that present no additional protective shell. Further confirmation of the successful introduction of Cu atoms in the bulk of the QD and their key role in the photophysics of the doped QDs is obtained through side-by-side photoluminescence experiments in the presence and in the absence of a strong hole-withdrawing agent, such as 1-dodecanthiol (DDT), following the approach introduced by Viswanatha *etal*. for the investigation of the recombination mechanism in Cu-doped ZnSe/CdSe QDs. (31) Specifically, the addition of a Lewis base, such as DDT, has been shown to dramatically quench the luminescence of undoped QDs by ultrafast extraction of photoexcited holes prior to radiative exciton recombination. (31) On the other hand, copper ions introduce intragap d-states close to the QD valence band that behave either as intrinsic hole-like states in the case of their substitutional incorporation as Cu^{2+} impurities (with d^9 electronic configuration) (31) or as efficient acceptors for photoexcited valence band holes when their oxidation state is +1 (corresponding to a filled d^{10} electronic shell). (79) In either situation, which most likely coexist in copper-doped QDs, (31, 34, 79) exposure of Cu:QDs to electron-rich moieties is inconsequential for the availability of hole-like states in the copper centers, leading to no luminescence quenching by nonradiative hole scavenging. On the other hand, the passivation effect by DDT of electron acceptor surface sites has been shown to significantly enhance the luminescence efficiency of Cu-doped QDs. Hence, the

positive *vs* negative photoluminescence response to the addition of DDT can be used to probe the presence of intragap copper states and, ultimately, to assess the successful incorporation of Cu impurities in the bulk of the semiconductor host. The data, reported in Figure S4, show nearly complete quenching of the luminescence of undoped QDs by efficient hole withdrawal by DDT and concomitant photobrightening of Cu:CdS QDs. This is in full agreement with the recombination mechanism of copper-doped QDs that involves the radiative relaxation of photoexcited electrons in impurity-related acceptor states, (77, 79) which are unaffected by ultrafast hole scavengers and that benefit from the passivating effect of surface electron traps by electron-donating moieties. (31) We finally stress that this behavior is consistent with the response of previously reported Cu:QDs obtained through growth doping methods where the dopants are incorporated in the bulk of the host lattice. (31) In our case, the seeded growth approach ensures that the dopant ions are originally positioned in the particle core and the low reaction temperature (35 °C) makes lattice diffusion and ejection processes unlikely to occur, as it was demonstrated for nucleation-doped Cu:ZnSe QDs, which required temperatures above 210 °C to activate self-purification mechanisms. (42)

Demonstration of Quantized Doping of Individual QDs

In order to quantitatively evaluate the doping level of individual QDs and to demonstrate that our approach yields uniform doping of the QD ensemble with the same number of dopant atoms per QD (corresponding to one Cu_4 cluster each), we

performed side-by-side elemental analysis by ICP-MS and XRF spectroscopy on the undoped and copper-doped CdS QDs produced in the excess of Cu_4 (hereafter indicated as Cu^{EX}:CdS) presented in Figure 2 and on a second Cu:QD sample we synthesized in the excess of QD precursors (Cu:CdS^{EX}). In combination with the elemental analysis, we performed spectrally and temporally resolved photoluminescence measurements that allow us to quantify, through their characteristic spectroscopic signatures, the relative populations of undoped and doped particles within the QD ensembles. By doing so for the Cu^{EX}:CdS QDs, we demonstrate that metal clusters effectively act as a "quantized" source for copper atoms and that a uniform population of doped QDs incorporating the equivalent of one cluster per dot can be easily synthesized at room temperature in water by operating in mild cluster excess conditions. Operating in excess of semiconductor precursors results instead in a bimodal distribution of two subpopulations of doped and undoped QDs. Importantly, the Cu:QDs obtained in the excess of QD precursors incorporate the atomic equivalent of one Cu_4 cluster per QD, similar to the Cu^{EX}:CdS QDs. Therefore, the copresence of doped and undoped QDs is, in this case, not accidental, but is a direct consequence of the quantized doping approach, where the number of available metal clusters in the reaction medium strictly determines the relative population of undoped *vs* homogeneously doped QDs. Figure 3a reports the contour plots of the time-resolved emission spectra of the undoped QD (top panel) in direct comparison with the two doped ensembles. In agreement with the data in Figure 2c,e, the photoluminescence of the undoped QDs is centered at 550 nm

(2.25 eV) and the signal decays completely within the first 250 ns. In contrast, the Cu^{EX}:CdS QDs (bottom panel) exhibit a much longer-lived emission at 610 nm, whose spectral position remains constant for over 2.5 µs, indicating that the solution is essentially a monodisperse population of doped particles. On the other hand, the $Cu:CdS^{EX}$ QDs show an intermediate behavior between the two limiting cases, with a fast high-energy spectral contribution due to undoped QDs accompanied by a slower emission at lower energy arising from the subpopulation of copper-doped QDs.

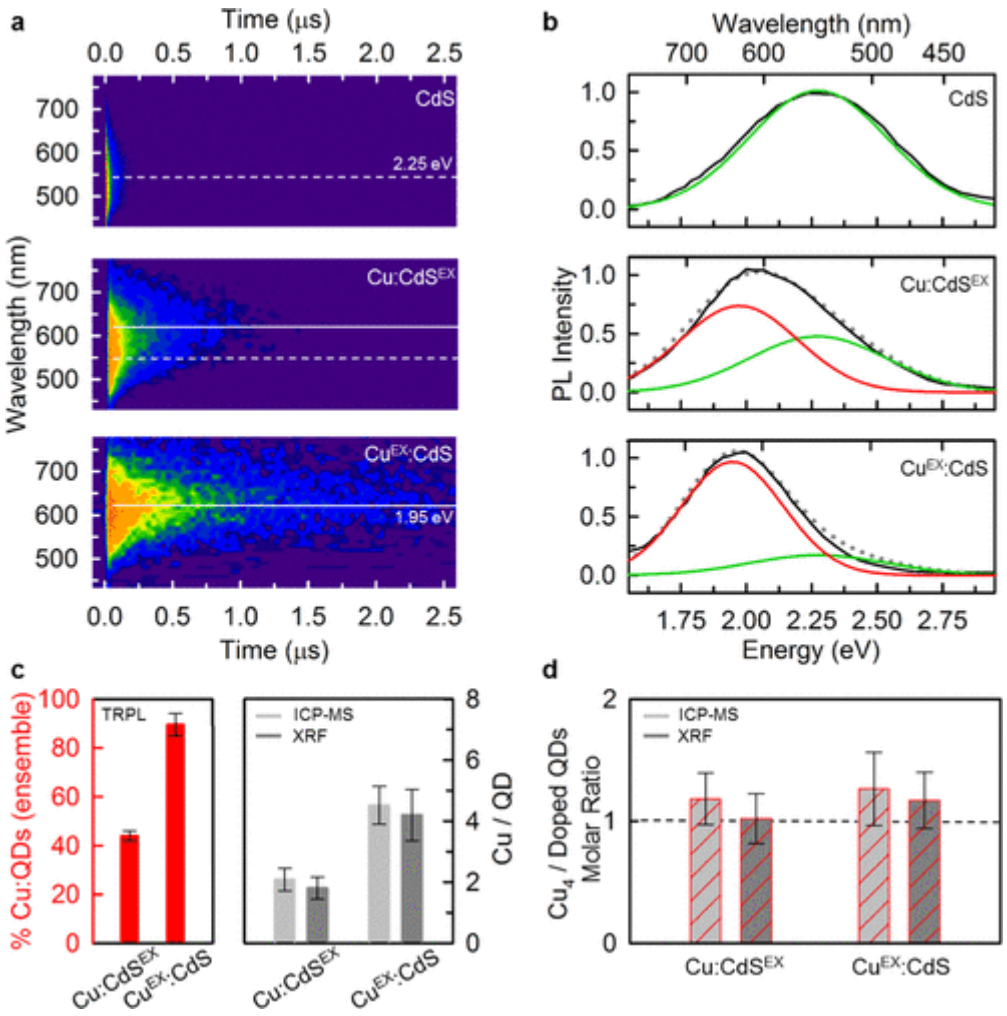

Figure 3. Quantitative demonstration of "quantized" QD doping. (a) Spectrally and time-resolved photoluminescence of stirred solutions of undoped and doped CdS QDs synthesized in an excess of QD precursors (Cu:CdS^{EX}) or in an excess of Cu_4 clusters (Cu^{EX}:CdS) under 365 nm pulsed excitation. (b) Continuous wave (cw) photoluminescence spectra of the same QDs as in (a) (black lines) and their deconvolution using a global fit with two spectral components, respectively ascribed to the subpopulation of doped dots (red curve, obtained by time integrating the time-resolved emission profiles of Cu^{EX}:CdS in (a) between 700 and 1500 ns) and undoped QDs (green curve, obtained by time integrating the time-resolved emission profiles of undoped dots in (a) between 0 and 50 ns). The global fit calculated as the sum of the two spectral components is shown as a dotted gray curve. (c) Left panel: Fraction of doped QDs in the Cu:CdS^{EX} and the Cu^{EX}:CdS ensembles extracted from the analysis time-resolved photoluminescence. Right panel: The average QD doping level estimated by ICP-MS and XRF spectroscopy. (d) Molar ratio between Cu_4 clusters and doped QDs calculated by combining the spectroscopic and the elemental analysis data. The results highlight that in both the Cu:CdS^{EX} and the Cu^{EX}:CdS ensembles each doped CdS QD contains four copper atoms, which corresponds to one Cu_4 cluster per QD.

In order to quantify the relative populations of doped and undoped particles in the two doped-QD ensembles, we deconvolved the respective continuous wave luminescence spectra using the emission profiles of undoped and doped QDs (Figure

3b), respectively extracted by integrating the time-resolved emission spectra of the CdS QDs in the t = 1–50 ns delay range and of the Cu^{EX}:CdS QDs for t = 700–1500 ns. The procedure, taking into account the comparable photoluminescence efficiency of undoped and doped particles (~4.5 ± 0.4%), yields a relative population of doped dots of ~45% in the Cu:CdS^{EX} QD ensemble and as high as ~95% for the Cu^{EX}:CdS QD sample. This confirms that the Cu_4 clusters act as nucleation seeds for doped QDs and that the spontaneous nucleation of undoped CdS particles occurs only in the excess of semiconductor precursors, that is, when the available clusters are insufficient in number to seed the growth of all CdS QDs. The quantitative elemental analysis by ICP-MS of the relative concentration of Cu and Cd atoms in the ensembles validates the original assumption that each QD contains one Cu_4 cluster, whose size determines the QD doping level. To demonstrate this aspect, we used the structural parameters provided by the TEM, XRD, and optical absorption reported in Figure 2 to estimate the average number of Cd atoms per QD—in the approximation of spherical particles—and compared the outcome to the average number of Cu atoms in the two doped QD samples (Figure 3c). This procedure for the Cu^{EX}:CdS QDs yields an average doping level of 4.5 ± 0.6 copper ions per dot, which, together with the essentially complete doping of the ensemble highlighted by the spectroscopic analysis (95% of the total QD population), proves that each CdS QD contains the equivalent of one Cu_4 cluster (Figure 3d).

The same conclusion is obtained also for the Cu:CdS^{EX} QDs, for which the elemental analysis indicates a Cu/QD ratio of ~2.1 ± 0.4, which, once scaled for the 45% population of doped particles in the ensemble (Figure 3c), yields 4.4 ± 0.5 copper atoms per doped QD, corresponding to a molar ratio of one Cu_4 cluster per doped QD (Figure 3d).

Finally, to independently confirm the doping levels in the two QD ensembles extracted from the ICP-MS analysis, we performed elemental analysis by XRF spectroscopy on both QD samples. Consistently with the mass spectroscopy data, the XRF results indicate a Cu/QD ratio of ~4.2 ± 0.8 and ~1.8 ± 0.4 for Cu^{EX}:CdS and Cu:CdS^{EX} QDs, respectively (Figure 3c). Also in this case, by scaling the average doping level for the respective population of doped *vs* undoped QDs in the ensembles, we obtain a molar ratio between Cu_4 cluster and doped QDs of 1.0 ± 0.2 and 1.1 ± 0.2 for Cu:CdS^{EX} and Cu^{EX}:CdS, respectively (Figure 3d), thus demonstrating the effectiveness of the proposed doping concept.

Conclusions

In summary, we demonstrated a strategy for controlling the doping level of QDs with atomic precision at the single-particle level, capable of producing homogeneously doped QD ensembles in which each particle contains the exact number of dopant atoms. This approach is based on the use of monodisperse colloidal metal particles acting as nucleation seeds for semiconductor QDs and providing a “quantum” of dopant atoms determined by their “magic size” that can

be pretuned by suitable choice of the cluster synthesis conditions. This approach effectively combines two traditionally orthogonal nanomaterial systems and potentially allows preselecting the doping of other semiconductor materials with various types of doping metals or alloys for achieving highly controlled doped QDs with tailored optoelectronic and magnetic functionalities.

Methods

Chemicals and Materials

Copper(II) nitrate, silver nitrate (≥99.9%), sodium borohydride (99.99%), 16-mercaptohexadecanoic acid (90%), L-glutathione (≥98%), sodium hydroxide (≥98%, pellets anhydrous), cadmium chloride (≥99.99%), tetrabutyl ammonium hydroxide solution (40% in water), sodium sulfide nonahydrate (≥98.0%), dodecanethiol (≥98%), methyl viologen dichloride hydrate (98%), ultrapure water (Chromasolv Plus, for HPLC), 2-propanol (≥99.8%), and ethanol (≥99.8%) were obtained from Sigma-Aldrich (Milan, Italy). D-Penicillamine (99%) was purchased from Alfa Aesar (Karlsruhe, Germany). All glassware was washed with *aqua regia* and rinsed with ultrapure water.

Synthesis of Undoped and Cu-Doped CdS Quantum Dots

Undoped CdS QDs

A 7 mL amount of 0.1 M tripeptide L-glutathione was added to 35 mL of ultrapure water in a two-necked flask under stirring followed by adjusting the pH to 10 by dropwise addition of an appropriate amount of 1.0 M NaOH solution. Next, 350 µL of 0.1 M $CdCl_2$ was added to the mixture and stirred for 5 min, after which 350 µL of 0.1 M Na_2S was injected. The reaction temperature was fixed to 35 °C, and the mixture was left to react for 3 h, after which the solution was purified using a 10 kDa centrifuge membrane to separate the QDs from the excess reactants.

Cu-Doped CdS QDs

To obtain Cu-doped CdS QDs, we followed the same synthesis route described for undoped CdS, with the only exception being the addition of 1.05 mL of Cu_4 clusters (4×10^{-2} M water solution) to the reaction medium (stated in the above procedure) for obtaining Cu^{EX}:CdS and 0.150 mL of Cu_4 clusters (4×10^{-2} M water solution) for obtaining Cu:CdS^{EX} QDs. After a 3 h reaction, the solution was purified and concentrated by passing through a 10 kDa centrifuge filter to completely remove the excess reactants and nonreacted Cu_4 clusters remaining in solution.

Cu Cluster Characterization

Electrospray Ionization Mass Spectrometry

ESI-MS experiments in positive-ion mode were performed on a hybrid quadrupole/time-of-flight instrument equipped with a nanoelectrospray ion source (AB Sciex, Foster City, CA, USA). The samples were infused by borosilicate-coated

capillaries of 1 µm internal diameter (Thermo Fisher Scientific, Waltham, MA, USA). The main instrumental parameters were as follows: ion-spray voltage 1.1 kV; curtain gas 20 psi; declustering potential 80 V. The recorded spectra were averaged over a 1 min acquisition time. The simulation of the peak distributions of the ESI-MS spectra was performed by IsoPro 3.1 based on the Yergey algorithm. (89)

X-ray Photoelectron Spectroscopy

The purified copper clusters were analyzed by means of XPS in order to investigate the oxidation states of the constituent metal atoms. Measurements were performed on a Kratos Axis Ultra^{DLD} spectrometer using a monochromatic Al Kα source operated at 15 kV and 20 mA. The specimen for XPS was prepared by drop casting 200 µL of a clean and concentrated sample solution onto a silicon wafer, thus obtaining a circular drop (approximately 1 cm wide in diameter) on it. All the analyses were carried out over an area of 300 × 700 µm. High-resolution analyses were carried out with a pass energy of 10 eV. The Kratos charge neutralizer system was used during data acquisition. Spectra have been charge corrected to the main line of the carbon 1s spectrum set to 284.8 eV (C–C bond). Spectra were analyzed using Casa XPS software (version 2.3.16).

Characterization of the Undoped and the Cu-Doped CdS QDs

High-Resolution Transmission Electron Microscopy

HR-TEM imaging was performed on a JEOL JEM-2200FS microscope equipped with a field emission gun working at an accelerating voltage of 200 kV, a CEOS spherical aberration corrector of the objective lens, allowing to reach a spatial resolution of 0.9 Å, and an in-column Omega filter.

Powder X-ray Diffraction

Powder XRD patterns were acquired in Bragg–Brentano geometry with Cu Kα radiation (Panalytical X'Pert Pro powder diffractometer).

Optical Measurements

Optical absorption spectra were recorded at room temperature on a Varian Cary 50 Scan UV–visible spectrophotometer. Figure S3 reports the analysis of the spectra of QD dispersions in water under normal incidence in quartz Suprasil cuvettes (optical path 0.1 cm).

Steady-state photoluminescence (PL) measurements were performed on a Cary Eclipse Varian fluorescence spectrophotometer at room temperature with a xenon lamp as a continuous wave light source. Time-resolved PL decays were recorded with an Edinburgh Instruments FLS 980 spectrofluorometer using a 405 nm EPL 405 (Edinburg Inst.) as excitation source (pulse width 40 ps). The luminescence quantum efficiency of CdS nanocrystals was determined by relative measurements in comparison with a 9,10 diphenylanthracene solution in deaerated tetrahydrofuran (10^{-6} M).

ICP-MS LA Spectrometry

The ICP-MS instrument is a PerkinElmer ELAN DRC-e. The LA (laser ablation) sampler is a New Wave UP 213 working with a quintupled Tempest laser at 213 nm. The protocol used for this analysis is based on the PerkinElmer proprietary semiquantitative method TOTALQUANT based on the instrument internal standardization. For this analysis, the internal standardization has been improved by a single measure of NIST 610, a glassy multielemental solid standard. Nanoparticles are measured after deposition and drying on a silica substrate from the liquid solution. Laser pulse energy was tuned in order to ablate the sample deposit, leaving undamaged the silica substrate. Due to the sulfur interfering signal and possible sulfur compound contamination of this solution, the method is considered reliable for the metal content, and the sum of the measured metal levels represents by definition 100% of the metallic mass. As a general consideration, the absolute error for this elemental analysis protocol could be estimated in the range ±25% for the majority of the elements. This error is mainly related to the uncertainty in the NIST 610 standardization procedure, and it is due to the NIST 610 composition uncertainty that has been estimated from the literature. (6) Due to the instrumental linearity range of 9 orders of magnitude and the stability, common for this kind of instrument, differently from an absolute measurement, the uncertainty of a relative measure between different samples showing the same matrix (if an internal

standard is available for the signal normalization between samples) is reliable within a few points of the percent of error.

Energy-Dispersive X-ray Fluorescence Spectroscopy (XRF)

Energy-dispersive XRF analysis was performed with a Bruker Artax 200 EDXRF spectrometer, equipped with an X-ray tube (Mo anode) with a beam collimated down to 0.65 mm in diameter. The induced characteristic X-ray fluorescence passes to a semiconductor detector, which works according to the drift chamber principle (silicon drift detector). A Mo transmission filter (12.5 μm thick) was used. The working conditions were 30 kV and 0.9 mA with an acquisition time of 1800 s for each measurement. Bruker Spectra 5.1 software was used to perform peak deconvolution. Element concentrations were obtained using reference materials with a stoichiometric concentration of the analytes and using sulfur as an internal standard. Specifically, CdS bulk single crystals were used to determine stoichiometric sulfur counts with respect to cadmium counts in QDs. $CuInS_2$ was adopted as stoichiometric standard to evaluate the copper content with respect to the stoichiometric counts of sulfur in CdS QDs. We performed three measurements in different areas of the same sample on a series of seven different samples to check the homogeneity and to evaluate the standard errors.

Acknowledgment

S.B. wishes to thank the European Community's Seventh Framework Programme (FP7/2007-2013) under grant agreement no. 324603 for financial support (EDONHIST). R.L., B.S.-G., and S.B. acknowledge support from Cariplo Foundation (2012-0844, 2012-0920).

(1) Kovalenko, M. V.; Manna, L.; Cabot, A.; Hens, Z.; Talapin, D. V.; Kagan, C. R.; Klimov, V. I.; Rogach, A. L.; Reiss, P.; Milliron, D. J.; Guyot-Sionnnest, P.; Konstantatos, G.; Parak, W. J.; Hyeon, T.; Korgel, B. A.; Murray, C. B.; Heiss, W. Prospects of Nanoscience with Nanocrystals. ACS Nano 2015, 9, 1012−1057.

(2) Pietryga, J. M.; Park, Y.-S.; Lim, J.; Fidler, A. F.; Bae, W. K.; Brovelli, S.; Klimov, V. I. Spectroscopic and Device Aspects of Nanocrystal Quantum Dots. Chem. Rev. 2016, 116, 10513−10622.

(3) Dai, X.; Zhang, Z.; Jin, Y.; Niu, Y.; Cao, H.; Liang, X.; Chen, L.; Wang, J.; Peng, X. Solution-Processed, High-Performance LightEmitting Diodes Based on Quantum Dots. Nature 2014, 515, 96−99.

(4) Shirasaki, Y.; Supran, G. J.; Bawendi, M. G.; Bulovic, V. Emergence of Colloidal Quantum-Dot Light-Emitting Technologies. Nat. Photonics 2013, 7, 13−23.

(5) Todescato, F.; Fortunati, I.; Minotto, A.; Signorini, R.; Jasieniak,J.; Bozio, R. Engineering of Semiconductor Nanocrystals for Light Emitting Applications. Materials 2016, 9, 672−700.

(6) Sargent, E. H. Colloidal Quantum Dot Solar Cells. Nat. Photonics 2012, 6, 133−135.

(7) Kagan, C. R.; Murray, C. B. Charge Transport in Strongly Coupled Quantum Dot Solids. Nat. Nanotechnol. 2015, 10, 1013−1026.

(8) Klimov, V. I.; Mikhailovsky, A. A.; Xu, S.; Malko, A.; Hollingsworth, J. A.; Leatherdale, C. A.; Eisler, H. J.; Bawendi, M. G. Optical Gain and Stimulated Emission in Nanocrystal Quantum Dots. Science 2000, 290, 314−317.

(9) Lorenzon, M.; Christodoulou, S.; Vaccaro, G.; Pedrini, J.; Meinardi, F.; Moreels, I.; Brovelli, S. Reversed Oxygen Sensing Using Colloidal Quantum Wells Towards Highly Emissive Photoresponsive Varnishes. Nat. Commun. 2015, 6, 6434.

(10) Medintz, I. L.; Uyeda, H. T.; Goldman, E. R.; Mattoussi, H. Quantum Dot Bioconjugates for Imaging, Labelling and Sensing. Nat. Mater. 2005, 4, 435−446.

(11) Bradshaw, L. R.; Knowles, K. E.; McDowall, S.; Gamelin, D. R. Nanocrystals for Luminescent Solar Concentrators. Nano Lett. 2015, 15, 1315−1323.

(12) Meinardi, F.; Colombo, A.; Velizhanin, K. A.; Simonutti, R.; Lorenzon, M.; Beverina, L.; Viswanatha, R.; Klimov, V. I.; Brovelli, S. Large Area Luminescent Solar

Concentrators Based on “Stokes-ShiftEngineered” Nanocrystals in Mass Polymerized Polymethylmethacrylate Matrix. Nat. Photonics 2014, 8, 392−399.

(13) Meinardi, F.; McDaniel, H.; Carulli, F.; Colombo, A.; Velizhanin, K. A.; Makarov, N. S.; Simonutti, R.; Klimov, V. I.; Brovelli, S. Highly Efficient Large-Area Colourless Luminescent Solar Concentrators Using Heavy-Metal-Free Colloidal Quantum Dots. Nat. Nanotechnol. 2015, 10, 878−885.

(14) Meinardi, F.; Ehrenberg, S.; Dhamo, L.; Carulli, F.; Mauri, M.; Bruni, F.; Simonutti, R.; Kortshagen, U.; Brovelli, S. Highly Efficient Luminescent Solar Concentrators Based on Earth-Abundant IndirectBandgap Silicon Quantum Dots. Nat. Photonics 2017, 11, 177−185.

(15) Krause, M. M.; Kambhampati, P. Linking Surface Chemistry to Optical Properties of Semiconductor Nanocrystals. Phys. Chem. Chem. Phys. 2015, 17, 18882−18894.

(16) Zhu, Z.-J.; Yeh, Y.-C.; Tang, R.; Yan, B.; Tamayo, J.; Vachet, R. W.; Rotello, V. M. Stability of Quantum Dots in Live Cells. Nat. Chem. 2011, 3, 963−968.

(17) Dubertret, B.; Skourides, P.; Norris, D. J.; Noireaux, V.; Brivanlou, A. H.; Libchaber, A. In Vivo Imaging of Quantum Dots Encapsulated in Phospholipid Micelles. Science 2002, 298, 1759−1762.

(18) Rossetti, R.; Ellison, J.; Gibson, J.; Brus, L. Size Effects in the Excited Electronic States of Small Colloidal CdS Crystallites. J. Chem. Phys. 1984, 80, 4464−4469.

(19) Brus, L. E. A Simple Model for the Ionization Potential, Electron Affinity, and Aqueous Redox Potentials of Small Semiconductor Crystallites. J. Chem. Phys. 1983, 79, 5566−5571.

(20) Brovelli, S.; Schaller, R. D.; Crooker, S. A.; García-Santamaría, F.; Chen, Y.; Viswanatha, R.; Hollingsworth, J. A.; Htoon, H.; Klimov,V. I. Nano-Engineered Electron-Hole Exchange Interaction Controls Exciton Dynamics in Core-Shell Semiconductor Nanocrystals. Nat. Commun. 2011, 2, 280.

(21) Donega, C. d. M. Synthesis and Properties of Colloidal Heteronanocrystals. Chem. Soc. Rev. 2011, 40, 1512−1546.

(22) Reiss, P.; Protiere, M.; Li, L. Core/Shell Semiconductor` Nanocrystals. Small 2009, 5, 154−168.

(23) Liu, S.; Borys, N. J.; Sapra, S.; Eychmüller, A.; Lupton, J. M. Localization and Dynamics of Long-Lived Excitations in Colloidal Semiconductor Nanocrystals with Dual Quantum Confinement. ChemPhysChem 2015, 16, 1663−1669.

(24) Todescato, F.; Minotto, A.; Signorini, R.; Jasieniak, J. J.; Bozio, R. Investigation into the Heterostructure Interface of CdSe-Based Core−Shell Quantum Dots Using Surface-Enhanced Raman Spectroscopy. ACS Nano 2013, 7, 6649−6657.

(25) Erwin, S. C.; Zu, L. J.; Haftel, M. I.; Efros, A. L.; Kennedy, T. A.; Norris, D. J. Doping Semiconductor Nanocrystals. Nature 2005, 436, 91−94.

(26) Norris, D. J.; Efros, A. L.; Erwin, S. C. Doped Nanocrystals. Science 2008, 319, 1776−1779.

(27) Jana, S.; Srivastava, B. B.; Jana, S.; Bose, R.; Pradhan, N. Multifunctional Doped Semiconductor Nanocrystals. J. Phys. Chem. Lett. 2012, 3, 2535−2540.

(28) Thuy, U. T. D.; Maurice, A.; Liem, N. Q.; Reiss, P. Europium Doped in(Zn)P/Zns Colloidal Quantum Dots. Dalton Trans. 2013, 42, 12606−12610.

(29) Molloy, J. K.; Lincheneau, C.; Karimdjy, M. M.; Agnese, F.; Mattera, L.; Gateau, C.; Reiss, P.; Imbert, D.; Mazzanti, M. Sensitisation of Visible and NIR Lanthanide Emission by InPZnS Quantum Dots in Bi-Luminescent Hybrids. Chem. Commun. 2016, 52, 4577−4580.

(30) Zhao, Y.; Rabouw, F. T.; Puffelen, T. v.; Walree, C. A. v.;Gamelin, D. R.; de Mello Donega, C.; Meijerink, A. Lanthanide-Doped CaS and SrS Luminescent Nanocrystals: A Single-Source Precursor Approach for Doping. J. Am. Chem. Soc. 2014, 136, 16533−16543.

(31) Viswanatha, R.; Brovelli, S.; Pandey, A.; Crooker, S. A.; Klimov, V. I. Copper-Doped Inverted Core/Shell Nanocrystals with “Permanent” Optically Active Holes. Nano Lett. 2011, 11, 4753−4758.

(32) Liu, J.; Zhao, Q.; Liu, J.-L.; Wu, Y.-S.; Cheng, Y.; Ji, M.-W.; Qian, H.-M.; Hao, W.-C.; Zhang, L.-J.; Wei, X.-J.; Wang, S.-G.; Zhang, J.-T.; Du, Y.; Dou, S.-X.; Zhu, H.-S.

Heterovalent-Doping-Enabled Efficient Dopant Luminescence and Controllable Electronic Impurity Via a New Strategy of Preparing II−VI Nanocrystals. Adv. Mater. 2015, 27, 2753−2761.

(33) Vlaskin, V. A.; Janssen, N.; van Rijssel, J.; Beaulac, R. m.; Gamelin, D. R. Tunable Dual Emission in Doped Semiconductor Nanocrystals. Nano Lett. 2010, 10, 3670−3674.

(34) Pandey, A.; Brovelli, S.; Viswanatha, R.; Li, L.; Pietryga, J. M.; Klimov, V. I.; Crooker, S. A. Long-Lived Photoinduced Magnetization in Copper-Doped ZnSe-CdSe Core-Shell Nanocrystals. Nat. Nanotechnol. 2012, 7, 792−797.

(35) Beaulac, R.; Schneider, L.; Archer, P. I.; Bacher, G.; Gamelin, D. R. Light-Induced Spontaneous Magnetization in Doped Colloidal Quantum Dots. Science 2009, 325, 973−976.

(36) Bussian, D. A.; Crooker, S. A.; Yin, M.; Brynda, M.; Efros, A. L.; Klimov, V. I. Tunable Magnetic Exchange Interactions in ManganeseDoped Inverted Core-Shell ZnSe-CdSe Nanocrystals. Nat. Mater. 2009, 8, 35−40.

(37) Rice, W. D.; Liu, W.; Pinchetti, V.; Yakovlev, D. R.; Klimov, V. I.; Crooker, S. A. Direct Measurements of Magnetic Polarons in Cd1−XMnxSe Nanocrystals from Resonant Photoluminescence. Nano Lett. 2017, 17, 3068.

(38) Mocatta, D.; Cohen, G.; Schattner, J.; Millo, O.; Rabani, E.; Banin, U. Heavily Doped Semiconductor Nanocrystal Quantum Dots. Science 2011, 332, 77−81.

(39) Kang, M. S.; Sahu, A.; Frisbie, C. D.; Norris, D. J. Influence of Silver Doping on Electron Transport in Thin Films of PbSeNanocrystals. Adv. Mater. 2013, 25, 725−731.

(40) Pradhan, N.; Goorskey, D.; Thessing, J.; Peng, X. An Alternative of CdSe Nanocrystal Emitters. J. Am. Chem. Soc. 2005, 127, 17586− 17587.

(41) Shao, P.; Zhang, Q.; Li, Y.; Wang, H. Aqueous Synthesis of Color-Tunable and Stable Mn2+-Doped ZnSe Quantum Dots. J. Mater. Chem. 2011, 21, 151−156.

(42) Chen, D.; Viswanatha, R.; Ong, G. L.; Xie, R.; Balasubramaninan, M.; Peng, X. Temperature Dependence of “Elementary Processes” in Doping Semiconductor Nanocrystals. J. Am. Chem. Soc. 2009, 131, 9333−9339.

(43) Jawaid, A. M.; Chattopadhyay, S.; Wink, D. J.; Page, L. E.; Snee, P. T. Cluster-Seeded Synthesis of Doped CdSe:Cu4 Quantum Dots.ACS Nano 2013, 7, 3190−3197.

(44) Hanif, K. M.; Meulenberg, R. W.; Strouse, G. F. Magnetic Ordering in Doped Cd1-xCoxSe Diluted Magnetic Quantum Dots. J. Am. Chem. Soc. 2002, 124, 11495−11502.

(45) Perera, S. D.; Zhang, H.; Ding, X.; Nelson, A.; Robinson, R. D. Nanocluster Seed-Mediated Synthesis of CuInS2 Quantum Dots, Nanodisks, Nanorods, and Doped Zn-CuInGas2 Quantum Dots. J. Mater. Chem. C 2015, 3, 1044−1055.

(46) Radovanovic, P. V.; Gamelin, D. R. Electronic AbsorptionSpectroscopy of Cobalt Ions in Diluted Magnetic Semiconductor Quantum Dots: Demonstration of an Isocrystalline Core/Shell Synthetic Method. J. Am. Chem. Soc. 2001, 123, 12207−12214.

(47) Mehra, S.; Bergerud, A.; Milliron, D. J.; Chan, E. M.; Salleo, A. Core/Shell Approach to Dopant Incorporation and Shape Control in Colloidal Zinc Oxide Nanorods. Chem. Mater. 2016, 28, 3454−3461.

(48) Sahu, A.; Kang, M. S.; Kompch, A.; Notthoff, C.; Wills, A. W.; Deng, D.; Winterer, M.; Frisbie, C. D.; Norris, D. J. Electronic Impurity Doping in Cdse Nanocrystals. Nano Lett. 2012, 12, 2587−2594.

(49) Eilers, J.; Groeneveld, E.; de Mello Donega, C.; Meijerink, A.́ Optical Properties of Mn-Doped ZnTe Magic Size Nanocrystals. J. Phys. Chem. Lett. 2012, 3, 1663−1667.

(50) Vlaskin, V. A.; Barrows, C. J.; Erickson, C. S.; Gamelin, D. R. Nanocrystal Diffusion Doping. J. Am. Chem. Soc. 2013, 135, 14380−14389.

(51) Barrows, C. J.; Chakraborty, P.; Kornowske, L. M.; Gamelin, D. R. Tuning Equilibrium Compositions in Colloidal Cd1−xMnxSe Nanocrystals Using Diffusion Doping and Cation Exchange. ACS Nano 2016, 10, 910−918.

(52) Yang, J.; Fainblat, R.; Kwon, S. G.; Muckel, F.; Yu, J. H.; Terlinden, H.; Kim, B. H.; Iavarone, D.; Choi, M. K.; Kim, I. Y.; Park,I.; Hong, H.-K.; Lee, J.; Son, J. S.; Lee, Z.; Kang, K.; Hwang, S.-J.; Bacher, G.; Hyeon, T. Route to the Smallest Doped Semiconductor: Mn2+-Doped (CdSe)13 Clusters. J. Am. Chem. Soc. 2015, 137, 12776−12779.

(53) Saha, A.; Shetty, A.; Pavan, A. R.; Chattopadhyay, S.; Shibata, T.; Viswanatha, R. Uniform Doping in Quantum-Dots-Based Dilute Magnetic Semiconductor. J. Phys. Chem. Lett. 2016, 7, 2420−2428.

(54) Fainblat, R.; Barrows, C. J.; Hopmann, E.; Siebeneicher, S.; Vlaskin, V. A.; Gamelin, D. R.; Bacher, G. Giant Excitonic Exchange Splittings at Zero Field in Single Colloidal CdSe Quantum Dots Doped with Individual Mn2+ Impurities. Nano Lett. 2016, 16, 6371− 6377.

(55) Bozyigit, D.; Lin, W. M. M.; Yazdani, N.; Yarema, O.; Wood, V. A Quantitative Model for Charge Carrier Transport, Trapping and Recombination in Nanocrystal-Based Solar Cells. Nat. Commun. 2015, 6, 6180.

(56) Nagpal, P.; Klimov, V. I. Role of Mid-Gap States in Charge Transport and Photoconductivity in Semiconductor Nanocrystal Films. Nat. Commun. 2011, 2, 486.

(57) Dance, I. G.; Choy, A.; Scudder, M. L. Syntheses, Properties,and Molecular and Crystal Structures of (Me4N)4[E4M10(SPH)16] (E= Sulfur or Selenium; M = Zinc or

Cadmium): Molecular Supertetrahedral Fragments of the Cubic Metal Chalcogenide Lattice. J. Am. Chem. Soc. 1984, 106, 6285−6295.

(58) Lees, E. E.; Nguyen, T.-L.; Clayton, A. H. A.; Mulvaney, P. The Preparation of Colloidally Stable, Water-Soluble, Biocompatible, Semiconductor Nanocrystals with a Small Hydrodynamic Diameter. ACS Nano 2009, 3, 1121−1128.

(59) Jing, L.; Kershaw, S. V.; Li, Y.; Huang, X.; Li, Y.; Rogach, A. L.; Gao, M. Aqueous Based Semiconductor Nanocrystals. Chem. Rev. 2016, 116, 10623−10730.

(60) Green, M.; Williamson, P.; Samalova, M.; Davis, J. J.; Brovelli, S.; Dobson, P.; Cacialli, F. Synthesis of Type II/Type I CdTe/CdS/ ZnS Quantum Dots and Their Use in Cellular Imaging. J. Mater. Chem. 2009, 19, 8341−8346.

(61) Zhang, L.; Wang, E. Metal Nanoclusters: New Fluorescent Probes for Sensors and Bioimaging. Nano Today 2014, 9, 132−157.

(62) Choi, S.; Dickson, R. M.; Yu, J. Developing Luminescent Silver Nanodots for Biological Applications. Chem. Soc. Rev. 2012, 41, 1867−1891.

(63) Chen, W.; Chen, S. In Functional Nanometer-Sized Clusters of Transition Metals: Synthesis, Properties and Applications; RSC: Cambridge, 2014.

(64) Qin, W.; Lohrman, J.; Ren, S. Magnetic and Optoelectronic Properties of Gold Nanocluster−Thiophene Assembly. Angew. Chem., Int. Ed. 2014, 53, 7316−7319.

(65) Corma, A.; Concepcion, P.; Boronat, M.; Sabater, M. J.; Navas, J.; Yacaman, M. J.; Larios, E.; Posadas, A.; Lopez-Quintela, M. A.; Buceta, D.; Mendoza, E.; Guilera, G.; Mayoral, A. Exceptional Oxidation Activity with Size-Controlled Supported Gold Clusters of Low Atomicity. Nat. Chem. 2013, 5, 775−781.

(66) Stamplecoskie, K. G.; Kamat, P. V. Size-Dependent Excited State Behavior of Glutathione-Capped Gold Clusters and Their Light Harvesting Capacity. J. Am. Chem. Soc. 2014, 136, 11093−11099.

(67) Santiago-Gonzalez, B.; Monguzzi, A.; Azpiroz, J. M.; Prato, M.; Erratico, S.; Campione, M.; Lorenzi, R.; Pedrini, J.; Santambrogio, C.; Torrente, Y.; De Angelis, F.; Meinardi, F.; Brovelli, S. Permanent Excimer Superstructures by Supramolecular Networking of Metal Quantum Clusters. Science 2016, 353, 571−575.

(68) Gonzalez, B. S.; Blanco, M. C.; Lopez-Quintela, M. A. Single Step Electrochemical Synthesis of Hydrophilic/Hydrophobic Ag5 and Ag6 Blue Luminescent Clusters. Nanoscale 2012, 4, 7632−7635.

(69) Wei, W.; Lu, Y.; Chen, W.; Chen, S. One-Pot Synthesis, Photoluminescence, and Electrocatalytic Properties of SubnanometerSized Copper Clusters. J. Am. Chem. Soc. 2011, 133, 2060−2063.

(70) Muhammed, M. A. H.; Aldeek, F.; Palui, G.; Trapiella-Alfonso, L.; Mattoussi, H. Growth of in Situ Functionalized Luminescent Silver Nanoclusters by Direct Reduction and Size Focusing. ACS Nano 2012, 6, 8950−8961.

(71) Jin, R. Atomically Precise Metal Nanoclusters: Stable Sizes and Optical Properties. Nanoscale 2015, 7, 1549−1565.

(72) Udayabhaskararao, T.; Sun, Y.; Goswami, N.; Pal, S. K.; Balasubramanian, K.; Pradeep, T. Ag7Au6: A 13-Atom Alloy Quantum Cluster. Angew. Chem., Int. Ed. 2012, 51, 2155−2159.

(73) Ganguly, M.; Jana, J.; Pal, A.; Pal, T. Synergism of Gold andSilver Invites Enhanced Fluorescence for Practical Applications. RSC Adv. 2016, 6, 17683−17703.

(74) Lesnyak, V.; Gaponik, N.; Eychmuller, A. Colloidal Semiconductor Nanocrystals: The Aqueous Approach. Chem. Soc. Rev. 2013, 42, 2905−2929.

(75) Gaponik, N.; Talapin, D. V.; Rogach, A. L.; Hoppe, K.; Shevchenko, E. V.; Kornowski, A.; Eychmüller, A.; Weller, H. ThiolCapping of CdTe Nanocrystals: An Alternative to Organometallic Synthetic Routes. J. Phys. Chem. B 2002, 106, 7177−7185.

(76) Kolny-Olesiak, J.; Weller, H. Synthesis and Application of Colloidal CuInS2 Semiconductor Nanocrystals. ACS Appl. Mater. Interfaces 2013, 5, 12221−12237.

(77) Brovelli, S.; Galland, C.; Viswanatha, R.; Klimov, V. I. Tuning Radiative Recombination in Cu-Doped Nanocrystals Via Electrochemical Control of Surface Trapping. Nano Lett. 2012, 12, 4372−4379.

(78) Meulenberg, R. W.; van Buuren, T.; Hanif, K. M.; Willey, T. M.; Strouse, G. F.; Terminello, L. J. Structure and Composition of CuDoped CdSe Nanocrystals Using Soft X-Ray Absorption Spectroscopy. Nano Lett. 2004, 4, 2277−2285.

(79) Srivastava, B. B.; Jana, S.; Pradhan, N. Doping Cu in Semiconductor Nanocrystals: Some Old and Some New Physical Insights. J. Am. Chem. Soc. 2011, 133, 1007−1015.

(80) Knowles, K. E.; Hartstein, K. H.; Kilburn, T. B.; Marchioro, A.; Nelson, H. D.; Whitham, P. J.; Gamelin, D. R. Luminescent Colloidal Semiconductor Nanocrystals Containing Copper: Synthesis, Photophysics, and Applications. Chem. Rev. 2016, 116, 10820.

(81) Jia, X.; Yang, X.; Li, J.; Li, D.; Wang, E. Stable Cu Nanoclusters: From an Aggregation-Induced Emission Mechanism to Biosensing and Catalytic Applications. Chem. Commun. 2014, 50, 237−239.

(82) Zhang, F.; He, X.-W.; Li, W.-Y.; Zhang, Y.-K. One-Pot Aqueous Synthesis of Composition-Tunable near-Infrared Emitting Cu-Doped CdS Quantum Dots as Fluorescence Imaging Probes in Living Cells. J. Mater. Chem. 2012, 22, 22250−22257.

(83) Sowa, H. On the Mechanism of the Pressure-Induced Wurtziteto NaCl-Type Phase Transition in CdS: An X-Ray Diffraction Study. Solid State Sci. 2005, 7, 73−78.

(84) Wu, P.; Yan, X.-P. Doped Quantum Dots for Chemo/Biosensing and Bioimaging. Chem. Soc. Rev. 2013, 42, 5489−5521.

(85) Xuan, T.; Wang, S.; Wang, X.; Liu, J.; Chen, J.; Li, H.; Pan, L.; Sun, Z. Single-Step Noninjection Synthesis of Highly Luminescent Water Soluble Cu+ Doped CdS Quantum Dots: Application as BioImaging Agents. Chem. Commun. 2013, 49, 9045−9047.

(86) Wei, H. H.-Y.; Evans, C. M.; Swartz, B. D.; Neukirch, A. J.; Young, J.; Prezhdo, O. V.; Krauss, T. D. Colloidal Semiconductor Quantum Dots with Tunable Surface Composition. Nano Lett. 2012, 12, 4465−4471.

(87) Yang, J.; Deng, D.-W.; Yu, J.-S. Transfer from Trap Emission to Band-Edge One in Water-Soluble CdS Nanocrystals. J. Colloid Interface Sci. 2013, 394, 55−62.

(88) Grandhi, G. K.; Tomar, R.; Viswanatha, R. Study of Surface and Bulk Electronic Structure of II−VI Semiconductor Nanocrystals Using Cu as a Nanosensor. ACS Nano 2012, 6, 9751−9763.

(89) Yergey, J. A. A General Approach to Calculating Isotopic Distributions for Mass Spectrometry. Int. J. Mass Spectrom. Ion Phys. 1983, 52, 337−349.